Polarization Dependent Water Adsorption on the Lithium Niobate Z-Cut Surfaces

S. Sanna, A. Riefer, M. Rohrmüller, M. Landmann, E. Rauls, N.J. Vollmers, R. Hölscher, M. Witte, Y. Li, U. Gerstmann, and W.G. Schmidt

Abstract The effect of ferroelectric poling on the water adsorption characteristics of lithium niobate Z-cut surfaces is investigated by ab initio calculations. Thereby we model the adsorption of H_2O monomers, small water clusters and water thin films. The adsorption configuration and energy are determined as a function of the surface coverage on both the positive and negative $LiNbO_3(0001)$ surfaces. Thereby polarization-dependent adsorption energies, geometries and equilibrium coverages are found. The different affinity of water to the two surfaces is explained in terms of different bonding scenarios as well as the electrostatic interactions between the substrate and the polar molecules. Surface phase diagrams for the Z-cuts in equilibrium with water are predicted from atomistic thermodynamics.

1 Introduction

Lithium niobate ($LiNbO_3$, LN) is one of the most important optic materials, being the equivalent in the field of non-linear optics and optoelectronics to silicon in electronics [1]. Recently the (microscopic) surface and interface properties have become important [2]. In particular, the polarization domains of ferroelectric oxide surfaces can be manipulated by an external electric field, in order to tailor the surface reactivity for specific applications. Indeed, polarization-dependent physical and chemical surface phenomena have been reported. Surface conductivity [3], threshold energy for photoelectron emission [4], thermally stimulated electron emission [5] and etching rate in acid solutions [6, 7] have been shown to be very different for differently polarized domains. Polarization-dependent adsorption of particle and molecules, either directly on the ferroelectric surface [8, 9] or on metal

S. Sanna · A. Riefer · M. Rohrmüller · M. Landmann · E. Rauls · N.J. Vollmers · R. Hölscher · M. Witte · Y. Li · U. Gerstmann · W.G. Schmidt (✉)
Lehrstuhl für Theoretische Physik, Universität Paderborn, 33095 Paderborn, Germany
e-mail: W.G.Schmidt@upb.de

W.E. Nagel et al. (eds.), *High Performance Computing in Science and Engineering '13*, DOI 10.1007/978-3-319-02165-2_12,

and semiconducting thin films deposited in a ferroelectric support [10], have been demonstrated too. In addition, photochemical deposition reactions can be combined with the local control of the ferroelectric polarization to drive the assembly of surface nanostructures [11]. Thus, domain engineering opens the possibility for the realization of molecular detectors and other devices at nanoscale level. In fact, it has been suggested that molecular adsorption may stabilize opposite poling directions in ferroelectric thin films, allowing for the realization of ferroelectric chemical sensors [12].

Water molecules have a prominent position among the common adsorbates, because of their role in natural phenomena such as catalysis, electrochemistry, corrosion and because of a variety of applications, including hydrogen production, fuel cells and biological sensors. Furthermore water will be present and influence the performance of the LN-based devices, unless they operate in ultra high vacuum (UHV). The functionality of devices might thus depend on the relative humidity. Indeed, water temperature programmed desorption (TPD) measurements at the positive and negative surface of $LiNbO_3$ indicate that the molecule-surface interaction are both coverage and polarization dependent. Another reason to study the water-LN interface is related to the fact that up to now high-resolution atomic force images of the LN surface could only be obtained in liquid environment [13].

Here we study the coverage dependent adsorption of water at the positive and negative LN(0001) surface [14] by means of atomistic simulations in the framework of the density functional theory (DFT). Adsorption energy, site and configuration are determined and the bonding between water and surface is analyzed and discussed. Surface thermodynamics is used to predict the ground state of water covered LN surfaces in dependence of temperature and pressure.

2 Methodology

Total energy density functional calculations have been performed within the PW91 formulation of the generalized gradient approximation (GGA) [15] as implemented in the VASP simulation package [16]. This approach allows for the accurate treatment of hydrogen bonds and water structures [17] and leads to reliable structures and energies for both LN bulk and surfaces [14, 18]. PAW potentials [19] with projectors up to $l = 3$ for Nb, $l = 2$ for Li, O and $l = 1$ for H, have been used for the calculations. The electronic wave functions are expanded into plane waves up to a kinetic energy of 400 eV.

Our work is based on the surface models proposed in [18, 20], which are in agreement with the experimental observation. According to these models, the positive surface is –Nb–O_3–Li_2 terminated, with one of the two top Li atoms relaxing down to the lower laying oxygen layer and the other above it, as represented in Fig. 1 (left). The negative surface is –Li–O terminated, instead (see Fig. 1 (right)). These models are used as basis for the investigation of the H_2O adsorption. Thereby we use slabs consisting of 18 atomic layers within a 2×2 periodicity (124 atoms

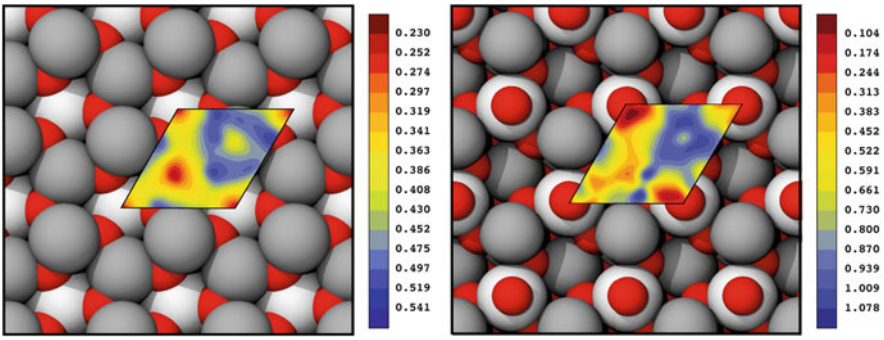

Fig. 1 PES for the adsorption of a single H_2O molecules on the positive (*left*) and negative (*right*) LN(0001) surface. Li atoms are *gray*, Nb *white* and oxygen *red*. Adsorption energies are in eV

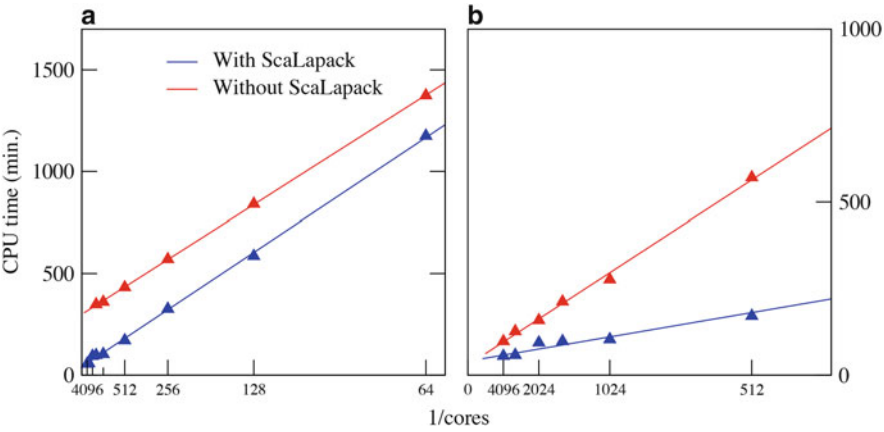

Fig. 2 CPU time required for a total energy calculation of stoichiometric $LiNbO_3$, modelled by a supercell containing 360 atoms and 2,160 electrons. (**a**) The effect of using the ScaLAPACK libraries in VASP. (**b**) Comparison between calculations performed by different simulation packages (VASP/*blue* and QuantumEspresso/*red*). The *blue* and the *red lines* are the linear interpolation of the calculated points and only serve to guide the eyes in order to appreciate the linear scaling at a first sight

for the positive face and 128 for the negative) and a vacuum region of ca. 16 Å. The lateral dimension of the unit cell largely reduces the unwanted interactions between the adsorbates and their periodic images. The dipole correction described in [21,22] has been used to correct the artificial forces generated by the slab images. A Γ-centered $2 \times 2 \times 1$ k-point mesh was used to carry out the integration in the Brillouin zone. The adsorbate and the 6 uppermost surface layers were allowed to relax until the forces were lower than 20 meV/Å.

Turning to the numerics, the density functional implementation used in the present study makes highly efficient use of the HLRS CRAY XE6, which presents the main computational resource for the present calculations. As shown in Fig. 2, the

scaling with the number of cores is roughly linear up to 4,096 cores. A substantial speedup is achieved by using the ScaLAPACK library. It is used for the LU decomposition and diagonalization of the sub space matrix, the dimension of which is given by the number of electronic states. These operations are very fast in the serial version, where they account for only about 2 % of the processor time, but become a bottleneck on massively parallel machines. While on slow networks and PC clusters, it is not recommended to use ScaLAPACK, it usage for the XE6 is obviously advantageous. In addition to the VASP simulation package [16], we also performed tests with the QuantumEspresso DFT implementation, parts of which were developed in our group [23]. Here we observe a superior scaling compared to VASP, although the total CPU time required is measurable larger, mainly due to the use of different pseudopotentials.

3 Results

We started our investigation with the determination of the favored adsorption site for single H_2O molecules on the considered model structure. We follow [18, 20, 24] concerning the convention for discriminating positive and negative surfaces. In a first step we have therefore calculated the potential energy surface (PES) for single adsorbates, which gives an approximate idea of the stable adsorption sites and a map of the different energy minima on the surface. Thereby we have evaluated the adsorption energy for 48 possible positions, and three different starting configurations, namely with the water dipole moment parallel, antiparallel and perpendicular to the spontaneous polarization of the substrate. The results are reported in Fig. 1 for the adsorption at the positive and negative side, respectively. The PESs are relatively corrugated, indicating a low surface mobility of the adsorbate. This holds in particular for the negative surface. Several minima and maxima of the adsorption energy are present at both sides. As a general feature, H_2O avoids a position right on top of the topmost Li atoms, and prefers an adsorption site between cations, above the lower lying oxygen atoms (second oxygen layer from the top).

In the energetically most favored configuration, the water molecule adsorbs tilted on the positive surface (see Fig. 3a) between one Li and one oxygen of the surface, with atomic distances $d(\mathrm{O{-}Li) = 2.06\,\text{Å}}$ and $d(\mathrm{O{-}H) = 1.76\,\text{Å}}$. Both the Li–O and O–H–O direction lie in the $(1\bar{1}00)$ plane. The water adsorption at the positive side does not substantially affect the substrate geometry. An analysis of the charge density reveals a polarization cloud between a water hydrogen and the surface oxygen it points to, as well as the negative charge accumulation at the oxygen side between molecule and surface Li (see Fig. 3a). The charge distribution, the interatomic distances and the adsorption geometry suggest that water molecules form both a Li–O bond of ionic character and an hydrogen-bond at the positive surface.

In the case of the negative surface the oxygen of the water molecule adsorbs close to a surface Li, at a distance $d(\mathrm{O{-}Li) = 1.83\,\text{Å}}$. One of the two hydrogen atoms

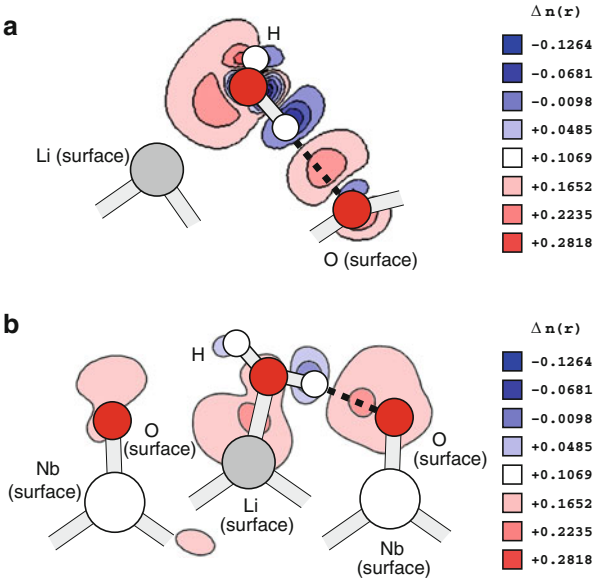

Fig. 3 Charge redistribution upon adsorption of the H_2O molecule at the positive (**a**) and negative (**b**) (0001) surface. Charge isolines in the $(1\bar{1}00)$ plane (which is y-plane as defined in [18]) are plotted. This plane contains the two bonds formed by the water molecule with the LN surface. *Red*/*blue* indicate regions with charge accumulation/depletion

points to a neighboring surface oxygen, with distance $d(\mathrm{O{-}H}) = 1.50\,\text{Å}$, while the other points out from the surface, as represented in Fig. 3b. Charge distribution, interatomic distances and geometry are compatible with a Li–O bond and a O–H hydrogen bond. The presence of the adsorbate induces some relaxation of the surface atoms. The adsorption pulls the surface Li out of its relaxed surface position and elongates its three bonds to neighboring oxygen ions. This is very similar to the effect of water adsorption at the non-polar $Al_2O_3(0001)$ surface, which was recently found to significantly disrupt the clean Al_2O_3 surface geometry [25]. We notice that another configuration of very similar energy can be created. In this case the oxygen of the water molecule again adsorbs close to a surface Li, at a distance $d(\mathrm{O{-}Li}) = 1.89\,\text{Å}$. However, both hydrogen atoms point roughly to a neighboring oxygen, with distances $d(\mathrm{O_1{-}H}) = 1.88\,\text{Å}$, and $d(\mathrm{O_2{-}H}) = 2.16\,\text{Å}$. In this second configuration all the water atoms are bound to the surface, with an ionic Li–O bond and two O–H hydrogen bonds (of different strength). In all the stable configurations, the z-component of the molecular dipole moment is directed against the spontaneous polarization of the substrate, thus reducing the total polarization.

The adsorption energy, as calculated from the difference

$$\mathrm{E_{ads}} = \mathrm{E_{slab}(H_2O@LN)} - \mathrm{E_{slab}(LN)} - \mathrm{E_{gas}(H_2O)} \tag{1}$$

amounts to 0.61 and 1.28 eV for the adsorption at the positive and negative surface respectively. The calculated energy difference is in qualitative agreement with

the temperature programmed desorption (TPD) measurements of Garra et al. [9]. However, the measured adsorption energy difference (estimated to be between 2.8 and 4.0 kJ/mol, corresponding to 0.029–0.041 eV) is lower than the values predicted by the theory (0.67 eV) by one order of magnitude. This discrepancy may partially be explained by the relatively large error bars affecting both the measurements and the calculations. At one side, the experimental value is obtained modeling the TPD spectra within the Polany–Wigner relations, which contain pre-exponential factors to be determined, and for which values scattered over several orders of magnitudes have been reported. It is also not clear to what extent the experimental preparation conditions result in the (thermodynamically stable) surface atomic structures supposed in our study. From the theoretical point of view it has to be said that adsorption energies do strongly depend on the parameterization of the exchange-correlation functional, both directly and indirectly through their geometry dependence. We mention that a recent theoretical study [26] on the adsorption of methanol on lithium niobate Z-cut surfaces also found larger adsorption energy differences between positive and negative surface than concluded from the experimental data. The sizeable adsorption energy difference calculated in this work can be understood from an atomistic and an electrostatic perspective. The disparity of the values can be traced back to the different bonding scenarios at the two faces. The bond at the negative Z-cut is shorter, i.e. stronger than at the positive surface. This is due to the different stoichiometries and the different morphologies of the two (0001) faces. From an electrostatic perspective, it must be considered that the work function at the positive Z-cut is by about 2 eV larger than at the negative surface [4, 18]. This could contribute to the difference in adsorption energy by affecting the electron transfer between molecule and surface, thus explaining why the H_2O adsorption at the negative side is favored with respect to the adsorption at the positive side.

Depending on the experimental conditions, surface adsorbed water may form different low-dimensional structures, ranging from isolated monomers and clusters to one-dimensional (1D) chains and two-dimensional (2D) overlayers (see, e.g. [27]). With increasing coverage, water may form networks of hydrogen-bonded molecules, water multilayers and bulk ice-like structures. In order to study the water adsorption at higher coverage, we systematically increased the number of water molecules up to 4 per surface unit cell. Different adsorption configurations as well as (partially) dissociated adsorption models were probed. A number of different structures have been found to be (meta)stable, the most relevant among them are shown in Figs. 4 und 5. At the positive surface, with two water molecules per unit cell, both highly regular honeycomb structures (similar to the water hexagons formed on many metal oxide or metal surfaces [25, 28]) or water chains (as observed on Rutile or ZnO [29]) have been found. They are shown in Fig. 4a, b, respectively. In both configurations the water hydrogen atoms point alternating to a surface oxygen and to the oxygen atom of the next water molecule. Three molecules per unit cell lead to the formation of a slightly distorted form of hexagons or chains plus an isolated water monomer. Four or more molecules per unit cell give rise to three-dimensional ice-like structures. The most stable of them are reminiscent of regular ice Ih.

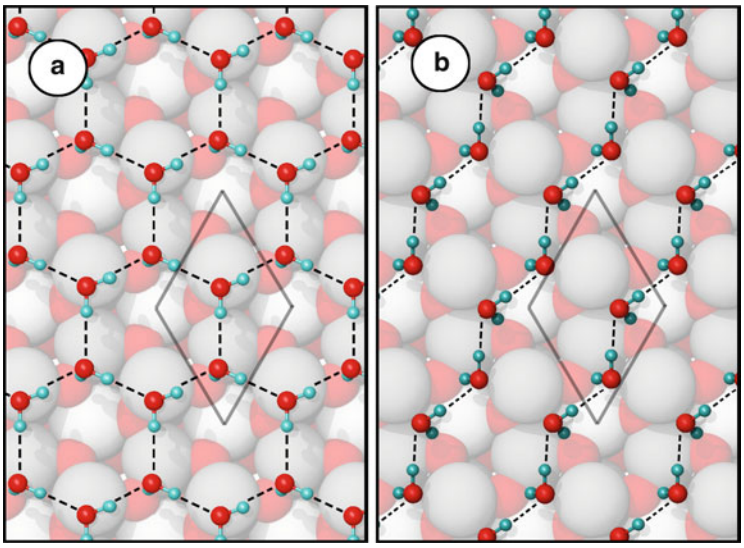

Fig. 4 Possible water configurations at the positive (0001) surface include (**a**) two dimensional regular hexagonal structures and chains (**b**). The rhombohedral unit-cell is highlighted

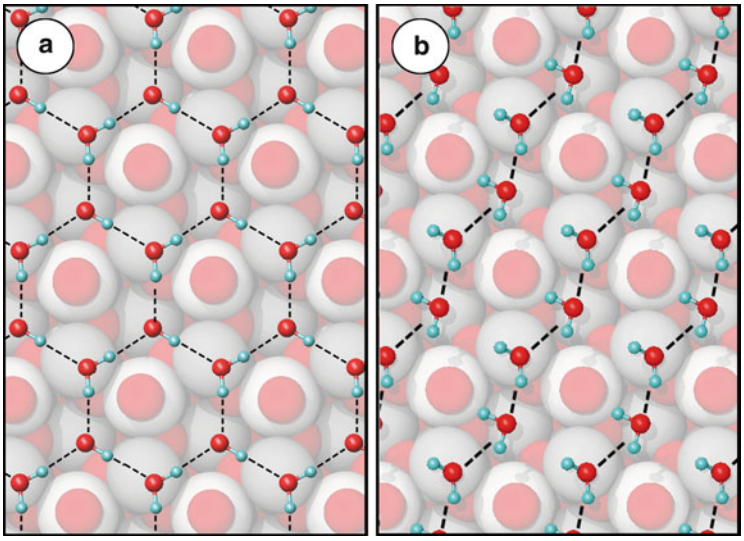

Fig. 5 Possible water reconstructions at the negative (0001) surface include two dimensional (**a**) hexamer structures and less regular chain structures

The negative (0001) surface is by far not as flat as the positive surface, it is rather characterized by a stronger surface corrugation. This hinders the uniform and regular adsorption of water films in regular patterns as in the case of the positive surface. Most of all, no more than two water molecules per unit cell can

be adsorbed. Increasing the number of water molecules results in the formation of ice layers separated from the surface (negative adsorption energy). Among the stable structures, honeycomb films and different kinds of distorted hexamers can be formed, as shown in Fig. 5. The dotted lines joining the water molecules are arbitrarily drawn guides for the eyes and do not represent a chemical bond. We remark that our adsorption models are based on ideal surfaces created in vacuum. Real surfaces will be characterized by steps and other surface defects (primarily oxygen and Li vacancies), by the presence of other adsorbates and, in case of extremely O-rich growth conditions, even by a different termination.

The particular water structure occurring on the LN surface depends on the water availability. To compare different surface water structures energetically, we use the thermodynamic grand-canonical potential

$$\Omega(\mu^{H_2O}) = F(n) - n\mu^{\mathrm{H_2O}} \approx E(n) - n\mu^{\mathrm{H_2O}}. \tag{2}$$

Here n is the number of water molecules and $F(n)$ the free energy of a surface with n adsorbed water molecules. In our work the free energy is approximated by the DFT total energy $E(n)$, which is a reasonable approximation if we assume similar entropy contributions for different adsorption configurations. The water chemical potential $\mu_{\mathrm{H_2O}}$ can be directly related to the experimental conditions. In the following $\Delta\mu_{\mathrm{H_2O}}$ refers to the difference between the water chemical potential $\mu_{\mathrm{H_2O}}$ and its value in the ice phase $\mu^{[\mathrm{ice}]}_{\mathrm{H_2O}}$. The dependence of $\Delta\mu_{\mathrm{H_2O}}$ on temperature and pressure can be calculated in the approximation of a polyatomic ideal gas [30] as

$$\Delta\mu_{\mathrm{H_2O}}(p,T) = k_B T \left[\ln\left(\frac{pV_Q}{k_B T}\right) - \ln Z_{\mathrm{rot}} - \ln Z_{\mathrm{vib}} \right], \tag{3}$$

where k_B is the Boltzmann constant, T the temperature and p the pressure. V_Q is the quantum volume and is equivalent to λ^3, whereby λ is the de Broglie thermal wavelength of the water molecule with mass m

$$\lambda = \sqrt{\frac{2\pi\hbar^2}{mk_B T}}. \tag{4}$$

Here

$$Z_{\mathrm{rot}} = \frac{(2k_B T)^{\frac{3}{2}}(\pi I_1 I_2 I_3)^{\frac{1}{2}}}{\sigma\hbar^3} \tag{5}$$

and

$$Z_{\mathrm{vib}} = \prod_{\alpha} \left[1 - \exp\left(-\frac{\hbar\omega_\alpha}{k_B T}\right) \right]^{-1} \tag{6}$$

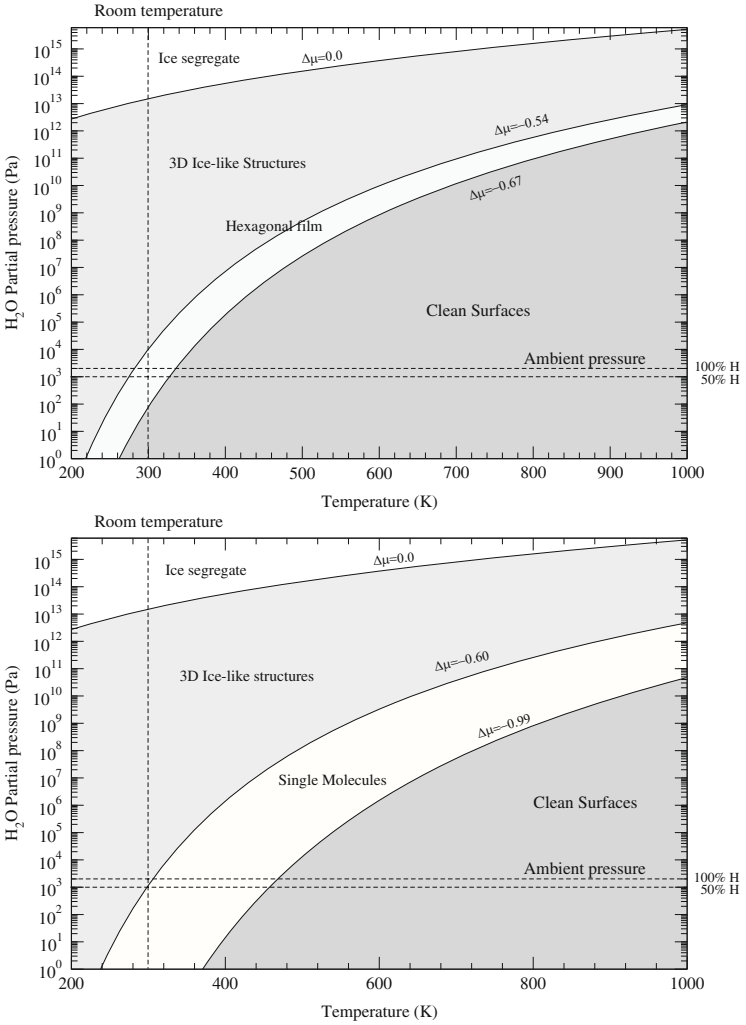

Fig. 6 Calculated phase diagram of the positive (*upper part*) and negative (*lower part*) $LiNbO_3(0001)$ surface as a function of the temperature and pressure. *Dotted lines* indicate the ambient conditions. The values of the chemical potential variations $\Delta\mu^{H_2O}$ (given with respect to ice Ih) at which a particular structure is formed, are indicated by *solid lines*

are the rotational and vibrational partition functions, respectively. We used the experimental values of the momenta of inertia I_i and of the vibrational frequencies ω_α of the water molecule [31]. The geometrical parameter σ takes the symmetry of the molecule into account. For H_2O (equal-sided triangle) it holds $\sigma = 2$. The calculated phase diagram of H_2O at the positive LN(0001) surface as a function of pressure and temperature is shown in Fig. 6 (top). According to our calculations,

a water film with hexagonal symmetry is present at the LN surface at ambient condition with a relative humidity of about 50 %. This is not surprising, as the adsorption of polar molecules is known to be the major external charge compensation mechanism [32]. Heating the system above 100 °C, clean LN (i.e. water free) surfaces are recovered. Increasing the water partial pressure above the room pressure leads to the growth of water bilayers and 3D-structures. At the negative side (Fig. 6, lower part) water monomers or ice seeds are present at ambient conditions. Our calculations predict a very interesting behavior: according to the phase diagrams in Fig. 6, water shall freeze at different temperatures on differently polarized LN surfaces. Indeed, this phenomenon has been experimentally observed recently for the isostructural ferroelectric $LiTaO_3$ [33].

Garra et al. have proposed that water adsorbs on the LN surfaces through a bonding interaction between each molecule's oxygen and a surface cation (Li, Nb), as well as through the electrostatic interaction between molecule's hydrogen atoms and oxygen atoms on the surface [9]. Our microscopic calculations clearly confirm/validate this model. In qualitative agreement with the experiment, the relative adsorption energy per water molecule decreases with the water coverage. The energetic difference between adsorption geometries is, however, smaller than 15 %. This indicates that the surface-molecule interaction is dominant over the molecule-molecule interaction. In further agreement with [9], the water adsorption is found to occur mainly non-dissociatively. To investigate this behavior the total energy of dissociated water molecules has been calculated in 30 different configurations at each side. Thereby water fragments have been positioned at the stable adsorption sites for O and OH radicals as calculated in [34]. At both sides the molecular adsorption was favored over the dissociated adsorption by at least 0.02 eV. However, the presence of different adsorbates in the atmosphere could modify the thermodynamic stability of the surfaces and favor dissociative adsorption. Furthermore, dissociative adsorption might occur close to a surface defect or in the vicinity of a step, as in the case of MgO(100) and other metal oxide surfaces [27, 35].

Regarding the electrostatics, the calculation of the work function upon adsorption yields insights into the charge compensation mechanisms, which play a crucial role in the physics of ferroelectric surfaces. Indeed, it allows us to determine the direction of the charge transfer between surface and adsorbates. An estimation of the surface charge of ideal, relaxed surfaces, can be found in [20]. The authors present a simple electrostatic model, predicting a positive charge of $+e/4$ at the LN$(000\bar{1})$ (so called negative surface) and a negative charge of $-e/4$ at the LN(0001) (so called positive surface). This charge is expected to be compensated by adsorbates. We predict a decrease of the work function (of 0.34 eV) at the negative side and an increase of the work function (of 0.49 eV) at the positive side upon adsorption of a single molecule. This corresponds to an electron transfer directed from the molecule to the surface at the positively charged side and vice versa from the surface to the adsorbate at the negatively charged surface. Thus, the water adsorption has in both cases a stabilizing influence as it reduces the surface charge.

4 Conclusions

We have performed density functional calculations to model the water adsorption at the $LiNbO_3$ surface. Isolated H_2O molecules are characterized by an adsorption energy of 0.61 and 1.28 eV at the positive and negative side, respectively. The adsorption configuration and adsorbate mobility are strongly polarization dependent, in qualitative agreement with temperature programmed desorption measurements [9]. The adsorption energy differences are due to different molecular bonding geometries on the two structurally distinct surfaces as well as different electrostatics. Various structures are formed with increasing water coverage, the adsorption energy per molecule of which is in qualitative agreement with the TPD data. Also in agreement with [9], the water adsorption is found to occur mainly non-dissociatively, independently on the coverage. At ambient condition and assuming a relative humidity of 50 %, we expect water molecules adsorbed at the LN(0001) surface, either in form of thin films with honeycomb symmetry or in small clusters.

Acknowledgements The calculations were done using grants of computer time from the Höchstleistungs-Rechenzentrum Stuttgart (HLRS) and the Paderborn Center for Parallel Computing (PC^2). The Deutsche Forschungsgemeinschaft is acknowledged for financial support.

References

1. A. Räuber, in *Chemistry and Physics of Lithium Niobate*. Current Topics in Materials Science (North-Holland Publ. Company, Amsterdam, 1978)
2. G. Namkoong, K.K. Lee, S.M. Madison, W. Henderson, S.E. Ralph, W.A. Doolittle, Appl. Phys. Lett. **87**(17), 171107 (2005)
3. Y. Watanabe, M. Okano, A. Masuda, Phys. Rev. Lett. **86**(2), 332 (2001)
4. W.C. Yang, B.J. Rodriguez, A. Gruverman, R.J. Nemanich, Appl. Phys. Lett. **85**(12), 2316 (2004)
5. B. Rosenblum, P. Bräunlich, J.P. Carrico, Appl. Phys. Lett. **25**(1), 17 (1974)
6. K. Nassau, H.J. Levinstein, G.M. Loiacono, J. Phys. Chem. Solids **27**, 983 (1966)
7. C.L. Sones, S. Mailis, W.S. Brocklesby, R.W. Eason, J.R. Owen, J. Mater. Chem. **295**, 12 (2002)
8. Y. Yun, L. Kampschulte, M. Li, a D. Liao, E.I. Altman, J. Phys. Chem. C **111**, 13951 (2007)
9. J. Garra, J.M. Vohs, D.A. Bonnell, Surf. Sci. **603**, 1106 (2009)
10. Y. Inoue, I. Yoshioka, K. Sato, J. Phys. Chem. **88**, 1148 (1984)
11. S.V. Kalinin, D.A. Bonnell, T. Alvarez, X. Lei, Z. Hu, J.H. Ferris, Q. Zhang, S. Dunn, Nano Lett. **2**(6), 589 (2002)
12. D.D. Fong, A.M. Kolpak, J.A. Eastman, S.K. Streiffer, P.H. Fuoss, G.B. Stephenson, C. Thompson, D.M. Kim, K.J. Choi, C.B. Eom, I. Grinberg, A.M. Rappe, Phys. Rev. Lett. **96**(12), 127601 (2006)
13. S. Rode, R. Hölscher, S. Sanna, S. Klassen, K. Kobayashi, H. Yamada, W. Schmidt, A. Kühnle, Phys. Rev. B **86**, 075468 (2012)
14. S. Sanna, R. Hölscher, W.G. Schmidt, Phys. Rev. B **86**, 205407 (2012)
15. J.P. Perdew, W. Yue, Phys. Rev. B **33**(12), 8800 (1986)
16. G. Kresse, J. Furthmüller, Phys. Rev. B **54**(16), 11169 (1996)
17. L. Giordano, J. Goniakowski, J. Suzanne, Phys. Rev. Lett. **81**, 1271 (1998)

18. S. Sanna, W.G. Schmidt, Phys. Rev. B **81**(21), 214116 (2010)
19. P.E. Blöchl, Phys. Rev. B **50**(24), 17953 (1994)
20. S.V. Levchenko, A.M. Rappe, Phys. Rev. Lett. **100**(25) (2008)
21. J. Neugebauer, M. Scheffler, Phys. Rev. B **46**(24), 16067 (1992)
22. L. Bengtsson, Phys. Rev. B **59**(19), 12301 (1999)
23. P. Giannozzi, S. Baroni, N. Bonini, M. Calandra, R. Car, C. Cavazzoni, D. Ceresoli, G.L. Chiarotti, M. Cococcioni, I. Dabo, A. Dal Corso, S. de Gironcoli, S. Fabris, G. Fratesi, R. Gebauer, U. Gerstmann, C. Gougoussis, A. Kokalj, M. Lazzeri, L. Martin-Samos, N. Marzari, F. Mauri, R. Mazzarello, S. Paolini, A. Pasquarello, L. Paulatto, C. Sbraccia, S. Scandolo, G. Sclauzero, A.P. Seitsonen, A. Smogunov, P. Umari, R.M. Wentzcovitch, J. Phys. **CM 21**(39), 395502 (2009)
24. R.S. Weis, T.K. Gaylord, Appl. Phys. A Mater. **37**(4), 191 (1985)
25. P. Thissen, G. Grundmeier, S. Wippermann, W.G. Schmidt, Phys. Rev. B **80**, 245403 (2009)
26. A. Riefer, S. Sanna, W.G. Schmidt, Phys. Rev. B **86**, 125410 (2012)
27. S. Meng, E.G. Wang, S. Gao, Phys. Rev. B **69**, 195404 (2004)
28. A. Michaelides, K. Morgenstern, Nat. Mater. **6**(8), 597 (2007)
29. O. Dulub, B. Meyer, U. Diebold, Phys. Rev. Lett. **95**, 136101 (2005)
30. L.D. Landau, E.M. Lifshitz, *Statistical Physics, Part I*, 3rd edn. (Butterworth-Heinemann, Oxford, 1981)
31. V.W. Laurie, D.R. Herschbach, J. Chem. Phys. **37**, 1687 (1962)
32. F. Johann, E. Soergel, Appl. Phys. Lett. **95**, 232906 (2009)
33. D. Ehre, E. Lavert, M. Lahav, I. Lubomirsky, Science **327**, 672 (2010)
34. R. Hölscher, S. Sanna, W.G. Schmidt, Phys. Stat. Sol. (c) **9**, 1361 (2012)
35. M.J. Stirniman, C. Huang, R.S. Smith, S.A. Joyce, B.D. Kay, J. Chem. Phys. **105**(3), 1295 (1996)